

Single-crystal diamond microwave devices for space applications

Original

Single-crystal diamond microwave devices for space applications / Russell, S. A. O.; Moran, D. A. J.; Verona, C.; Limiti, E.; Cappelluti, Federica; Ghione, Giovanni; Barnes, A.. - ELETTRONICO. - (2014), pp. 154-157. (9th European Microwave Integrated Circuits Conference, EuMIC 2014 - Held as Part of the 17th European Microwave Week, EuMW 2014 Fiera di Roma, ita 2014) [10.1109/EuMIC.2014.6997815].

Availability:

This version is available at: 11583/2658599 since: 2018-05-04T12:03:12Z

Publisher:

Institute of Electrical and Electronics Engineers Inc.

Published

DOI:10.1109/EuMIC.2014.6997815

Terms of use:

This article is made available under terms and conditions as specified in the corresponding bibliographic description in the repository

Publisher copyright

IEEE postprint/Author's Accepted Manuscript

©2014 IEEE. Personal use of this material is permitted. Permission from IEEE must be obtained for all other uses, in any current or future media, including reprinting/republishing this material for advertising or promotional purposes, creating new collecting works, for resale or lists, or reuse of any copyrighted component of this work in other works.

(Article begins on next page)

Single-Crystal Diamond Microwave Devices for Space Applications

S.A.O.Russell,
D.A.J.Moran
University of Glasgow,
Glasgow, UK

C.Verona, E.Limiti
Università di Roma Tor
Vergata, EE / IE Depts.
Roma, ITALY

F.Cappelluti, G.Ghione
Politecnico di Torino, DET
Dept.
Torino, ITALY

A.Barnes
ESA-ESTEC
Noordwijk,
The Netherlands

David.Moran@glasgow.ac.uk

limiti@ing.uniroma2.it

giovanni.ghione@polito.it

Andrew.Barnes@esa.int

Abstract—The physical operation, crystal growth, optical lithography and electron-beam lithography fabrication and measured performance of single-crystal diamond active devices for microwave frequencies are presented. Preliminary results suggest the potentials of such technology in high-frequency and power operation. The use in space applications is envisaged, thanks to the peculiar diamond features to operate in harsh environments and with remarkable RF performance.

Keywords—Single-crystal, diamond active devices, microwave high power.

I. INTRODUCTION

Diamond contains several attractive physical and electrical properties making it an excellent candidate for many electronic applications.

The wide band gap, small electron affinity, high saturation drift velocity, high carrier mobility, radiation hardness and high thermal conductivity make diamond, together with GaN [1] a promising material for fabrication of high power, high frequency and high temperature solid-state microelectronic devices, especially for use under adverse conditions and in harsh environment [2], [3].

The exceptional material properties of diamond are summarized in Figure 1 [4], [5]. The wide band gap in diamond is responsible for the high breakdown field and low intrinsic carrier concentration. Extremely high thermal conductivity in diamond results from fast relaxation times of acoustic phonons, allowing very fast heat dissipation during the operation of high power electronic device made of this material [6].

As compared to other small band gap semiconductors materials like silicon, the use of diamond, leads to many advantages. An electronic device made of diamond can operate at high fields and temperatures whereas silicon based devices experience crystal damage when operated at high temperature due to increased diffusion of impurities in the crystal.

The large dielectric constant and consequently large capacitance of silicon-based devices, in contrast to diamond, increase the time response of such electronic device.

All of the above properties make diamond an ideal candidate for high-frequency, high-power applications in harsh environments, and, in particular, for space-based transmitter subsystems, where diamond-based transistors could ultimately replace vacuum tube devices.

Johnson's figure of merit [7] of diamond, an indicator of a semiconductor's suitability for high-frequency high-power devices, is the highest among semiconductors.

Semiconductor Materials		Diamond	Si	Ge	6H-SiC
Structural Properties	Lattice constant (Å)	3.567	5.431	5.658	a: 3.081 c: 15.117
	Density (gcm ⁻³)	3.52	2.33	5.33	3.22
Thermal Properties	Melting point T _m (K)	4100 ^{<2>}	1687	1210.4	2810
	Specific heat C _p (Jg ⁻¹ K ⁻¹)	0.51	0.71	0.33	0.58
	Debye temperature θ _D	1870	643	348	1126
	Thermal expansion coefficient α ₀ (10 ⁻⁶ K ⁻¹)	1.05	2.616	5.75	α _z : 4.2 α _c : 4.7
	Thermal conductivity (K)	22	1.56	0.6	4.9 ^{<2>} 3.30 ^{<3>}
Elastic Properties ^{<4>}	Young's modulus (GPa)	1148.2	157.2	126.8	c // f: 4.73 c // t: 5.44
	Poisson's ratio	0.068	0.21	0.195	c // f: 0.14 c // t: 0.09
	Knoop microhardness (GPa)	56–115	2–16	9.92	21.3–27.6
Lattice Dynamic Properties	Long-wavelength optical phonon frequencies $\hbar\omega_{LO}$ (cm ⁻¹)	1332	519.2	301	965
	Optical phonon frequency difference $\Delta\omega_{LO} = \omega_{LO} - \omega_{TO}$ (cm ⁻¹)	0	0	0	167
Electronic properties	Indirect bandgap (eV)	5.50	1.12	0.67	3.00
	Electron Affinity (eV) [36] ^{<5>}	H: -1.30 O: 1.73	4.05	4.14	3.34
	The breakdown field (10 ⁵ Vcm ⁻¹) in Schottky barriers and p-n junctions	>200 ^{<6>}	3	1	24
	Electron mobility (cm ² V ⁻¹ s ⁻¹)	2800	1750	2300	375
	Hole mobility (cm ² V ⁻¹ s ⁻¹)	1500	450	2400	100
	Electron saturation velocity (10 ⁷ cm.s ⁻¹)	1.5	1.02	0.7	1.9
	Hole saturation velocity (10 ⁷ cm.s ⁻¹)	1.1	0.72	0.63	NA
	Intrinsic resistivity (Ωcm) [37]	>10 ⁻³	10 ⁷	47	>10 ⁻¹
	Dielectric constant	5.7	11.9	16.0	10
Optical Properties	Refractive index	2.4	3.4	4	2.55
Biological properties [33]		excellent	NA	NA	NA
Chemical resistance [33]		excellent	NA	NA	NA

Figure 1: Fundamental properties for principal semiconductors at 300 K.

Clearly technology readiness level is at the moment not compatible with the target applications and therefore a technological assessment has to be performed to make diamond technology effective. In this contribution the single-crystal diamond growth, the lithographic realization, the operating physical principles and compact modelling of the resulting active devices are presented, together with the preliminary

experimental results. The research efforts are deployed within the frame of a TRP project financed by the European Space Agency with the aim to assess diamond technology for space applications.

II. OPERATING PRINCIPLE AND COMPACT MODELING

Hydrogen-terminated (H-terminated) diamond MESFETs use the two-dimensional hole gas (2DHG) formed underneath the hydrogenated diamond surface as a conductive channel, whose sheet carrier density is controlled by a Schottky gate contact realized by a low workfunction metal (typically Al) deposited on the H-terminated diamond surface. The source and drain ohmic contacts are made by high workfunction metals, such as Au. Both enhancement- and depletion-like behavior has been demonstrated, depending on the specific fabrication technology.

There is almost general consensus on the origin of surface hole accumulation in H-terminated diamond samples exposed to atmosphere: adsorbate molecules are considered responsible for the transfer of electrons from the diamond valence band to the 2DHG and for the subsequent formation of the 2DHG (the so-called surface-transfer doping model). However, the exact physical behavior of Schottky contacts on H-diamond still is an open question. I/V and C/V characteristics as well as microstructural characterizations suggest the formation of a nonconductive interfacial layer (IL), a few nm thick, separating the 2DHG from the gate contact and providing, with the gate metal, a potential barrier for holes [8].

Channel formation could be then explained by the generation of a dipole layer related to adsorbates at the diamond surface (with similarity to the piezoelectric induced channel in AlGaN-GaN HEMTs) [9], or by a transfer doping effect from diamond valence band to acceptor centers located in the interfacial layer (with similarity to a modulation doping mechanism), or by a combination of the two.

Despite such uncertainties, compact modelling strategies are worth being developed, with the aim to support further investigation on the physics and morphology of the Schottky contacts and to provide a physical basis to the development of specific equivalent large-signal circuit models. In order to develop a physics-based charge-control model of the Al/H-diamond contact, both the above mentioned mechanisms (adsorbate-induced polarization and transfer doping) can be modelled by using a delta-like charge layer in the IL as schematically shown in the inset of Figure 2. An example of simulated C-V curves are reported in Figure 2, for a postulated structure with physical parameters that were estimated from the experimental I/V and C/V characteristics measured on large area Schottky samples ($d_{IL} = 5.5$ nm, $q\Phi_B = 1.5$ eV, $\Delta E_V = 0.5$ eV).

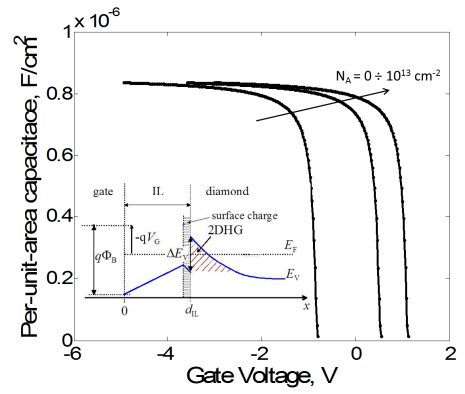


Figure 2: Example of simulated C-V curves for different concentration of IL/diamond surface charge (N_A). The inset sketches the valence band energy alignment at the IL-diamond interface.

The simulated behaviour is representative of typical C/V curves also reported in literature. In the example, the enhancement- or depletion-like behaviour of the 2DHG charge control can be modelled by tuning the density of the net (negative) surface charge, N_A , located at the IL/diamond interface.

The numerical charge control model is then exploited to evaluate the MESFET DC and quasi-static small-signal characteristics, by using well known quasi-2D approaches developed for the physic-based analysis of III-V and III-N HEMTs. An example of comparison between simulated and measured DC I/V characteristics of a device with gate length of 200 nm (see [10] for device details) is shown in Figure 3, proving the effectiveness of the approach. Based on these promising results, large-signal nonlinear circuit models based on the Chalmers approach have been recently successfully applied to the simulation of surface channel H-terminated diamond MESFETs both on polycrystalline and single-crystal substrates [11].

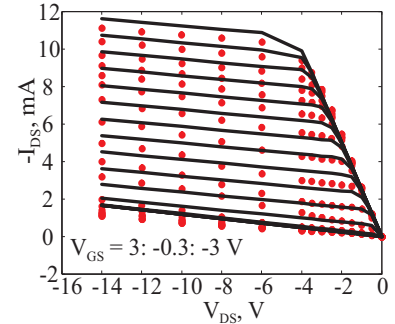


Figure 3: Measured (symbols) and simulated (solid line) DC characteristics of H-terminated diamond FET with $L_g = 200$ nm described in [10].

III. CVD DIAMOND GROWTH AND HYDROGENATION

High-quality intrinsic single crystal diamond films with a thickness of about 1 μ m were homo-epitaxially grown by the MWPECVD technique explained above, onto $4.5 \times 4.5 \times 0.5$ mm³ commercial low-cost synthetic High Pressure High Temperature (HPHT) type Ib single-crystal diamond substrates, procured from Element 6 (E6). Several samples have been grown. The intrinsic diamond typical growth conditions was the following: substrate temperature about 650 °C, chamber pressure 90 Torr, microwave power

600 W, methane (CH_4) and hydrogen (H_2) flow rates 1 and 100 sccm respectively. Purity of CH_4 and H_2 gases are 99.9995 % and 99.9999 % respectively. The single crystal intrinsic diamonds were grown keeping constant the microwave power during the growth. All CVD diamond films have been then characterized by X-ray diffraction, Scanning Electron Microscopy (SEM), Atomic Force Microscope (AFM) and Time of Flight Secondary Ion Mass Spectrometry (TOF-SIMS) confirming the single crystal homo-epitaxial deposition, the good crystal quality and good surface morphology of the grown samples.

Prior to fabricating any test device, the diamond surface has to be terminated with hydrogen (H-termination), in order to form a p-type channel. H-surface termination was performed by exposing the diamond surface to H plasma in situ, i.e. in the same microwave CVD reactor at the end of the growth.

In particular, the following procedure was followed: stop CH_4 gas flow and expose the diamond film to hydrogen plasma for about 20 min; turn off the microwave power and cool down the substrate to room temperature in a pure hydrogen atmosphere. Experimental results have shown that, in order to minimize the structural and morphological defects (especially on the surface), the temperature of the diamond samples during the growth should be in the range between 600-700 °C. Within such interval, substantial differences have not been observed. Moreover, since the temperature is monitored by an optical pyrometer, an error of the temperature of about ± 10 °C is expected due to the different reflectivity of diamond substrates.

In order to increase the conductance (or the hole sheet concentration) of hydrogenated diamond surface, exposure to a specific gas (O_3 , NO_2 , NO , SO_2) is necessary. In the present case, NO_2 is adopted: The adsorption process of NO_2 on H-terminated diamond surface starts soon after a background pressure of 10^{-2} mbar is achieved.

X-Ray diffraction measurements were performed by means of a Bragg-Brentano diffractometer utilizing the K_α line ($\lambda = 1.541$ Å) as incident radiation. From the measurement, a lattice constant of our diamonds of 3.567 Å has been computed. The FWHM of the rocking curve is fully accounted for by the diffractometer resolution confirming the single crystal homo-epitaxial deposition and the good crystal quality of the grown samples. Morphological characterization and investigation of diamond surface films grown is carry out by SEM images. the diamond surface is free of defects like pyramidal hillocks, flat hillocks, and unepitaxial crystallites. Residual impurities and crystalline defects in the bulk and on the surface can affect active device operation. However, isolated pits of about 1 μm can be found on diamond surface. Such pits, called “etch-pits”, are created by the etch of Hydrogen plasma during the growth. In order to investigate the formation of C-H bond on diamond surface, the H-terminated diamond samples previously covered with gold were analyzed by TOF-SIMS (Time-Of-Flight Secondary Ion Mass Spectrometry). Primary ion bombardment was carried out with 30 kV Bi^+ ions.

IV. OPTICAL LITHOGRAPHY PROCESSING

On the basis of past experience on polycrystalline diamond devices [12], before any fabrication was undertaken, a 100 nm Au ‘sacrificial layer’ was evaporated on to the samples. Then, a series of optical lithography masks were used to define devices with different gate peripheries (finger length) and resulting in a gate length of about 1.2 μm . In the following Figure 4, a SEM image of the Drain-Source region of a sample FET device is reported (left) together with an optical microscope image of the entire processed sample (right).

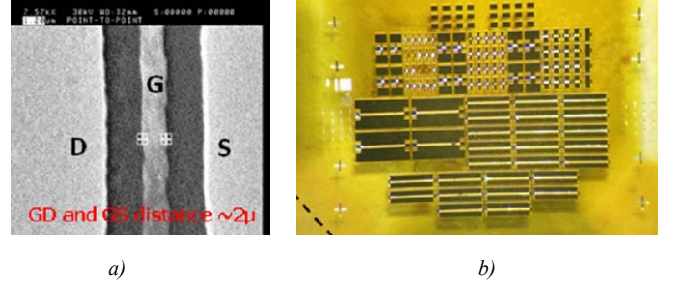


Figure 4: a) SEM image of 1 μm gate length; b) Optical microscope image of top view of diamond devices.

The resulting devices were DC tested to extract the device static performance. As an example, in the following Figure 5 the I/V curves of a sample 2 x 10 μm device are plotted.

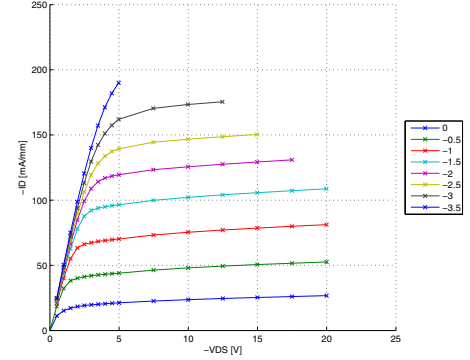


Figure 5: Measured I/V curves of a 2 x 10 μm device. Drain current density vs V_{DS} , with V_{GS} as a parameter.

Also RF performance of the devices has been tested for the differed peripheries. As an example, power gain and current gain versus frequency for a 50 μm gate periphery device is plotted in the following Figure 6.

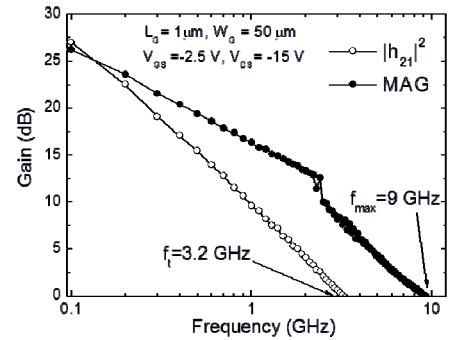


Figure 6: Current and power gain as functions of frequency for a 2 x 25 μm device.

As it can be noted, an f_{MAX} of about 9 GHz and f_T of over 3 GHz have been achieved. It is to note that such frequency performance is a remarkable one if the 1.2 μm gate length is considered.

VI. CONCLUSION

The physical operation, crystal growth, optical lithography and electron-beam lithography fabrication and measured performance of single-crystal diamond active devices for microwave frequencies have been briefly presented. The preliminary measured results demonstrate the viability of such technology in high-frequency and power operation and space application. Further achievements will be illustrated in the final contribution.

ACKNOWLEDGMENT

The support of the European Space Agency under contract No. 4000107749/13/NL/RA is gratefully acknowledged.

REFERENCES

- [1] V.Teppati, V.Camarchia, S.Donati Guerrieri, M.Pirola, A.Ferrero, G.Ghione, M.Peroni, P.Romanini, C.Lanzieri, S.Lavanga, A.Serino, E.Limiti, L.Mariucci, "Fabrication and Nonlinear Characterisation of GaN HEMT on SiC and Sapphire for High Power Applications," International Journal on RF and Microwave Computer-Aided Engineering, Vol.16, n°1, January 2006, pp.70-80.
- [2] J.E.Field, Properties of Diamond, Academic, London, 1979.
- [3] J.Prins, "Applications of diamond films in electronics," in The Physics of Diamond, A.Paoletti and A.Tucciarone (editors), Amsterdam, IOS Press (1997) 411.
- [4] S.Adachi, Properties of Group-IV, III-V and II-VI Semiconductors. Materials for electronic & optoelectronic Applications, 2005, Wiley.
- [5] S.Pan Lawrence, Diamond: Electronic Properties and Application. Electronic Material: Science & Technology, 1994, Springer.
- [6] A.Rossani, "Generalized Kinetic theory of electrons and phonons: models equilibrium and stability," Physica B, 334, 2003, 292.
- [7] E.O.Johnson, "Physical limitations on frequency and power parameters of transistors," RCA Review, Vol.26, 1965, pp.163.
- [8] M.Kasu et al., "Gate interfacial layer in hydrogen-terminated diamond field-effect transistors," *Diamond and Rel. Mat.*, Vol.17, 2008, pp.741-744.
- [9] K.Hirama et al., "Spontaneous polarization model for surface orientation dependence of diamond hole accumulation layer and its transistor performance," *APL*, 92.11 (2008): 112107-112107.
- [10] V.Camarchia et al., "RF power performance evaluation of surface channel diamond MESFETs," *Solid-State Electronics*, Vol.55, n.1, 2011, pp.19-24.
- [11] V.Camarchia et al., "Accurate large-signal equivalent circuit of surface channel diamond FETs based on the Chalmers model," *Diamond and Rel. Mat.*, Vol.26, n.6, 2012, pp.15-19.
- [12] P.Calvani, A.Corsaro, M.Girolami, F.Sinisi, D.M.Trucchi, M.C.Rossi, G.Conte, S.Carta, E.Giovine, S.Lavanga, E.Limiti, V.Ralchenko, "DC and RF Performance of Surface Channel MESFETs on H-Terminated Polycrystalline Diamond," *Diamond and Related Materials*, Vol.18, n°5-8, January 2009, pp.786-788.
- [13] S.A.O.Russell, S.Sharabi, A.Tallaire, D.A.J.Moran, "Hydrogen-terminated diamond field-effect transistors with cutoff frequency of 53 GHz," *IEEE EDL*, vol.33, no.10, pp.1471-1473, Oct.2012.
- [14] S.A.O.Russell, L.Cao, D.Qi, A.Tallaire, K.G.Crawford, A.T.S.Wee, D.A.J.Moran, "Surface transfer doping of diamond by MoO_3 : A combined spectroscopic and Hall measurement study," *APL*, vol.103, pp.202112-1-4, Nov.2013.

V. ELECTRON BEAM LITHOGRAPHY & PASSIVATION

Along with the large gate periphery useful for high power FET operation, gate length scaling can lead to improved RF frequency performance assuming parasitic resistances can be scaled accordingly.

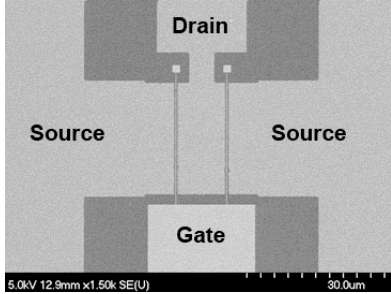


Figure 7: SEM Image of RF layout for hydrogen-terminated diamond FET.

Recently a hydrogen-terminated diamond FET with 50 nm gate length has been demonstrated achieving a cutoff frequency of 53 GHz [13]. This performance makes diamond a promising material for producing devices for space and radar applications. To operate in the extreme environment of space however it is essential to stabilize the 'surface transfer doping' process which provides charge carriers in this material. Hydrogen-terminated diamond possesses a negative electron affinity so electron transfer will occur between the surface and a suitable high electron affinity acceptor material such as atmospheric molecules to give a sub-surface p-type doping. A suitable passivation for the surface transfer doping process has long been sought after to provide stable device operation at high voltages and over a range of temperatures. Recent progress has been made in this regard whereby the deposition of MoO_3 on to hydrogen-terminated diamond has been shown to not only preserve but even enhance the doping efficiency [14]. Figure 8 demonstrates the improvement in sheet resistance which may arise from deposition of MoO_3 on to a hydrogen-terminated diamond surface after baking to remove atmospheric adsorbate molecules. The sheet resistance decreased from a value of 7065 Ω/\square to 3791 Ω/\square immediately after deposition.

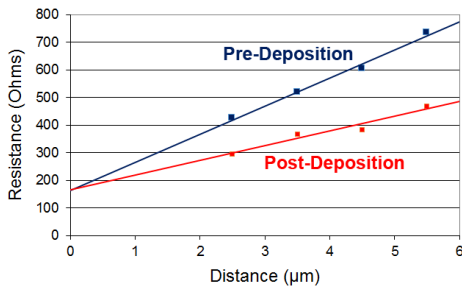


Figure 8: Resistance obtained from TLM structures before and after MoO_3 deposition